10536 *Macromolecules* **2010**, *43*, 10536–10544
DOI: 10.1021/ma1018846

Macromolecules
ARTICLE

# Effects of Composition, Orientation and Temperature on the $O_2$ Permeability of Model Polymer/Clay Nanocomposites

**Erik Dunkerley and Daniel Schmidt***

*Department of Plastics Engineering, University of Massachusetts Lowell, 1 University Avenue, Lowell, Massachusetts 01854, United States*

*Received August 17, 2010; Revised Manuscript Received October 22, 2010*

ABSTRACT: Studies of the barrier properties of polymer/layered silicate nanocomposites have traditionally focused on systems with low organoclay contents, with very little work comparing theory and experiment over broad composition ranges. As a result, in spite of many reports of promising enhancements in barrier properties, the envelope of applicability nanocomposite barrier models is generally unknown, making predictive modeling and materials design difficult if not impossible. In this work, model polystyrene (PS)/dimethyl ditallow modified montmorillonite (DMDT-MMT) nanocomposites are produced via a novel spray casting technique capable of creating homogeneous, free-standing nanocomposite films. This approach provides a single experimental methodology for producing films of pure polymer, pure organoclay, or any intermediate composition, with consistently high levels of layer orientation in all cases. The results of oxygen permeation analysis (OPA) performed on these model materials (0−100 vol % organoclay in 10% increments) are compared to the results from all models commonly used for nanocomposite barrier properties modeling, both before and after the addition of a correction factor for actual layer orientation as measured by 2D wide-angle X-ray diffraction (WAXD), and with fitting parameters limited to physically meaningful values. We report substantial improvements in barrier properties in spite of the absence of exfoliation, with the model fits implying that the permeating species remain sensitive to the aspect ratio of individual platelets at all organoclay contents. While all models match our experimental data at low organoclay contents, significant differentiation occurs as organoclay content is increased. Finally, we confirm that the permeability of these materials follows an Arrhenius relation vs temperature, albeit scaled to lower values as a function of inorganic content.

## Introduction

Understanding and enhancing the barrier properties of nanocomposites and the effects of tortuosity on diffusion has long been a focus of the nanocomposite community.[1−4] Adding even a few weight percent of a platy nanofiller such as a nanoclay has been shown to improve the barrier properties in nearly every case, so long as good dispersion is achieved.[1,5] In particular, montmorillonite is preferred for nanocomposite work due to its low cost, high aspect ratio, and low toxicity and its ability to be modified with alkylammonium surfactants to achieve dispersibility.[6] Understanding and extending the range of applicability of mathematical models for nanocomposite barrier properties is critical to further realizing the benefits and identifying the limitations of nanocomposite barrier materials.

While the majority of work on nanoclay barrier films has been on low nanoclay content melt-processed materials, typically with 10 wt % nanoclay or less, some work has been done on high inorganic content films, demonstrating that further improvements in barrier properties are achievable. A number of manufacturing methods for high nanoclay content composites have been successfully applied, including spray deposition of solutions on to substrates,[7,8] layer by layer assembly,[9,10] and bottom up colloidal assembly.[11] Spray deposition shows promise as a means of producing uniform, well-oriented films of arbitrary composition, making it an ideal approach for producing nanocomposites for barrier modeling.

A number of models have been applied to describe the permeation behavior of nanolayer-based composites. However, due to the limited work in nanocomposites with clay concentrations above 10 wt %, in general these models have not been challenged to describe permeation trends over the full range of possible compositions. This is a critical point, because it means that the range of applicability of these models has not been identified experimentally and remains unknown.

Classic rule-of-mixtures approaches analogous to those of Reuss and Voigt for mechanical behavior[12] establish the upper and lower bounds of permeation but do not predict behavior well in the case of particulate composites, due to the fact that these models were not designed to deal with discrete filler particles. This prompted the development of classic (Nielsen[13]) and reflective tortuosity (Cussler[14,15]) models, which describe the effects of the filler on barrier properties by assuming the presence of regular or randomly spaced arrays of perfectly aligned impermeable ribbons or flakes with a certain aspect ratio associated with their cross-section. The advent of nanolayer-based composites has inspired the development of two additional models based on the work of Gusev and Lusti,[16] (an empirical fit of the results of finite element modeling) and Fredrickson and Bicerano,[17] (a first principles model based on disk-shaped inclusions), respectively, which treat randomly spaced arrays of perfectly aligned disk-shaped platelets. It is clear, however, that the assumption of perfect alignment is problematic when X-ray diffraction measurements of orientation in organoclay nanocomposites always indicate otherwise.[18] Eitzman, Melkote, and Cussler attempt to address this issue at filler loadings below 20 vol % both experimentally and via Monte Carlo simulations,[19] while Bharadwaj offers a theoretical treatment of the Nielsen model for classic tortuosity modified to include an orientation parameter.[20] This parameter ranges from

*Corresponding author. E-mail: Daniel_Schmidt@uml.edu.

 Published on Web 12/06/2010 

a value of −0.5 for a system, where the long axis of the filler is oriented parallel to the permeation direction (no tortuosity), to a value of 1, where it is oriented perpendicular to the permeation direction (maximum tortuosity), with a value of 0 representing random orientation. Conveniently, this is analogous to the behavior of the Hermans orientation parameter often derived from 2D X-ray diffraction results. This factor allows a weighted average to be made between the zero tortuosity state (where permeation is reduced via reductions in permeant solubility only) and the maximum tortuosity state (where the model's tortuosity factor comes into play). While Bharadwaj does not offer a strict first-principles derivation of his approach, the earlier work of Eitzman, Melkote, and Cussler[19] presents a mathematically identical correction factor for orientation and shows that it effectively describes the results of both Monte Carlo simulations and experimental results from mica flake based macrocomposites with a highly regular structure. In the latter case, the only difference stems from the fact that the authors did not present their solution as a function of Hermans orientation parameter, but instead as a function of orientation angle. The fact that this one approach to orientation correction has been successfully applied in multiple settings demonstrates its relevance, while the utility of stating the relationship in terms of Hermans orientation parameter as a practical means of accounting for experimental data on orientation levels in real samples is readily apparent. The ability to do so represents a key correction, and while further improvements are certainly possible, this approach represents an improvement over the assumption of perfect orientation the use of other models implies.

Here a series of nanocomposites consisting of polystyrene and dimethyl ditallow modified montmorillonite (DMDT-MMT) is described. These components were chosen due to the fact that polystyrene is amorphous (changes in crystalline microstructure may confound the results) and able to spontaneously form a thermodynamically favored intercalated structure in the presence of DMDT-MMT when provided sufficient mobility to do so. Polystyrene is also compatible with solvents capable of dispersing DMDT-MMT,[21−23] relevant for packaging applications, and well studied in the research literature in combination with this high aspect ratio nanoclay.[24−34] Thin, free-standing films from this family of materials were produced via a novel spray deposition process and characterized with respect to composition via thermogravimetric analysis (TGA), structure via scanning electron microscopy (SEM) and 2D wide-angle X-ray diffraction (WAXD), and barrier properties via oxygen permeation analysis (OPA). The oxygen permeation data was then compared to one of the four aforementioned permeation models, both as originally stated and including a correction for platelet orientation. Finally, while increases in temperature are known to result in an Arrhenius-type exponential increase in permeation in polymer films,[35,36] such behavior has not been studied in nanocomposites. As such, additional oxygen permeation analyses were carried out at selected compositions as a function of temperature to complete the picture of barrier properties variations in this model nanocomposite system.

## Experimental Section

**Film Preparation.** Achieving dispersion is critical to producing consistent samples and relevant data; few processing techniques, however, are able to achieve that goal over the entire range of nanoclay contents from 0 to 100%. A solution based technique[37−39] was chosen for this work entailing dispersing DMDT-MMT (Southern Clay Products Cloisite 20A) and dissolving polystyrene (Scientific Polymer #845, $M_w = 190\,000$ g/mol) in toluene via mixing with a Teflon-coated magnetic stir bar overnight at room temperature. Films were formed by spraying the resultant mixture onto FEP release film. A standard air powered spray gun (Husky HDS550) with a 1.8 mm (0.071 in.) nozzle i.d. was used to atomize the solution and apply it to the film, which was mounted on a rotating drum. The speed of the surface as it moved past the spray gun was approximately 0.22 m/s. The nozzle of the spray gun was set at an approximate angle of 90° vs the surface and a distance of approximately 20 cm from the drum. Compressed nitrogen was used to operate the gun at a pressure of 207 kPa (30 psi). For the film to have enough strength to be demolded in one piece, multiple coats were applied to build up the film thickness to 0.06 to 0.27 mm. The surface often remained wet for up to 30 s after the coating was applied. Care was taken, however, not to apply too much material too quickly, since that was found to result in cracking. After each coat was applied, the surface was allowed to dry for 70 s allowing it to become dry to the touch. All samples were the further dried at 125 °C for 4 h in a convection oven to remove residual solvent and relieve any residual stresses trapped during the film formation process. This method was preferred over traditional casting due to the improvement in processing time and control and the reduction in defects such as cracking during drying.

**Scanning Electron Microscopy.** Cross sectional scanning electron micrographs were taken to ascertain film thickness and composite morphology. Films were freeze fractured in liquid $N_2$ to expose their cross sections and subsequently mounted vertically, fractured cross-section up, in a custom-built SEM holder. The film cross sections were observed in either an environmental SEM (Quanta 600F, FEI, Hillsboro, OR) or a high resolution Hitachi field emission SEM at various magnifications. All samples were coated with gold−palladium using a desktop gold sputter coater and imaged with an accelerating voltage of 2.0−5.0 kV.

**X-ray Diffraction.** Wide angle X-ray diffraction (WAXD) measurements were performed using a Statton box camera and a Cu Kα source generated with a Rigaku ultraX system. The sample to detector distance was set to 193 mm for all samples unless otherwise noted. The detector consisted of a reusable X-ray sensitive image plate that was scanned to create a 2-dimensional digital image of the X-ray diffraction pattern. All samples were tested under vacuum to minimize scattering due to air, and were oriented edge-on, with the incident beam parallel to the plane of the film. The digital image was analyzed using FIT2D v12.077 for Windows to produce 2-theta and azimuthal integration plots in order to quantify interlayer spacing and degree of orientation utilizing Bragg's law and the Hermans orientation parameter, respectively. Interlayer spacing was measured by using the Θ angle at which the first and second order diffraction peaks occurred and averaging the results. Orientation was measured by using data from 0 to 90 deg in the azimuthal scan of the second order diffraction peak to avoid the influence of the nonlinear background intensities observed around the first order peak as well as artifacts near the beam stop.

**Oxygen Permeation Analysis.** Oxygen permeation analysis (OPA) was performed using an Illinois instruments Model 8001 oxygen permeation analyzer. Two simultaneous analyses were performed on separate samples of each composition studied at 23 °C and 0% RH. Ultra high purity nitrogen and oxygen were used for all purging and analyses. Each sample was mounted so as to cover a 25 mm diameter hole in a solid brass masking plate, and the instrument was purged with nitrogen to an initial oxygen concentration of ∼0.14 ppm in the nitrogen carrier gas stream (equivalent to an oxygen transmission rate of 4 $cm^3/m^2 \cdot$day, as set in the instrument software) prior to the introduction of oxygen on the opposite side of the sample. The sampling interval used was 60 min and the test was set to terminate following three consecutive readings from the same sample within ±1% of one another, consistent with steady-state conditions. Typical testing times varied from 18 to 24 h. The oxygen permeation rate was then calculated by multiplying the measured transmission rate by the average sample thickness. Each sample was measured at five points oriented in a cross pattern over the testing area using a dial

**Table 1. Desired Composition, Inorganic Content (from TGA) and Orientation Parameter and Interlayer Spacing (from WAXD) of DMDT-MMT/Polystyrene Nanocomposites**

| DMDT-MMT content (vol %) | | | inorganic content (wt %) | | | |
|---|---|---|---|---|---|---|
| theoretical | actual | inorganic content (vol %) | theoretical | actual | orientation parameter | interlayer spacing (nm) |
| 100 | 100 | 37.9 | 61.2 | 61.2 | 0.68 | 2.30 |
| 90 | 89.2 | 34.1 | 57.4 | 57.1 | 0.72 | 2.79 |
| 80 | 79.3 | 30.3 | 53.3 | 53.0 | 0.73 | 3.42 |
| 70 | 70.3 | 26.5 | 48.8 | 48.9 | 0.79 | 3.33 |
| 60 | 60.7 | 22.7 | 43.8 | 44.2 | 0.76 | 3.31 |
| 50 | 50.7 | 18.9 | 38.4 | 38.8 | 0.76 | 3.34 |
| 40 | 40.8 | 15.1 | 32.4 | 32.9 | 0.74 | 3.36 |
| 30 | 30.8 | 11.4 | 25.7 | 26.3 | 0.73 | 3.34 |
| 20 | 21.3 | 7.6 | 18.1 | 19.1 | 0.69 | 3.36 |
| 10 | 10.3 | 3.8 | 9.7 | 9.9 | 0.67 | 3.37 |
| 0 | 0 | | | | | |

micrometer with a precision of 0.001 mm, and the results were averaged. The average film thickness was found to be between 0.06 and 0.27 mm for the nanocomposites described here, with typical standard deviations on the order of 0.002−0.05. In order to examine the effect of temperature on permeability the temperature of the cell was adjusted in 5 °C increments from 20 to 50 °C. At each temperature, the permeation rate was allowed to stabilize until readings were within ±1% of one another. After the highest temperature was tested, the apparatus was allowed to cool back to 20 °C and the sample reanalyzed to determine whether the increase observed was reversible.

**Thermogravimetric Analysis.** Thermogravimetric analysis (TGA) was conducted on each batch of material using a TA Instruments Q50 thermogravimetric analyzer. For all tests, a platinum pan was used, and samples were heated at 20 °C/min to a maximum temperature of 850 °C. In all cases, this was high enough to give a plateau indicative of complete removal of all organic/volatile matter. Samples were analyzed in ultra zero air at 60 mL/min while the balance gas was ultra high purity nitrogen with a flow rate of 40 mL/min. The nonvolatile content was compared to the inorganic content of the nanoclay alone to determine how close each sample was to the desired composition.

**Nonlinear Regression Method.** OriginLab Origin Pro 8 was used to perform all nonlinear regression analysis of the data using the various permeation models, with the inorganic content (in vol %) as the independent variable and the oxygen permeation rate (in $cc \cdot mm/m^2 \cdot day$) as the dependent variable. The fitting procedures used allowed for variations in the oxygen permeability of the pure polymer, the aspect ratio of the platelets and the orientation parameter of the nanolaminate as a whole, but only within physically reasonable bounds. A Levenberg−Marquardt algorithm was used to adjust the parameters to maximize the fit. For aspect ratio the lower and upper bounds were set to 0 and 150, respectively (the latter being the maximum stated by the organoclay manufacturer), to allow for the possibility that the formation of stacks would result in a reduction in effective aspect ratio, as is often assumed in the literature. The bounds for $P_o$ were 195 to 197 based on the measured value for pure polystyrene film prepared in the same way as the nanocomposites described here and accounting for the standard deviation of the measurement. Finally, the bounds for the orientation parameter were 0.67 and 0.79, the lower and upper limits of the orientation parameters measured by 2D wide-angle X-ray diffraction, respectively. All coefficients of determination ($r^2$) were adjusted to compensate for the number of terms within the models.

## Results and Discussion

Accurately modeling and understanding the permeation behavior of the nanocomposite materials described here first requires a detailed understanding of their composition and morphology. Following film formation, TGA was performed to confirm the compositions of the hybrids as well as the removal of residual solvents, with the results shown in Table 1. The measured weight fraction of inorganic material present in the nanocomposites can be converted to volume fraction of organoclay using the measured weight fraction of inorganic in the neat organoclay in tandem with the manufacturer's stated densities for the neat polystyrene[40] (1.05 g/cm$^3$), the neat DMDT-MMT[41] (1.77 g/cm$^3$) and the "unmodified" ($Na^+$) MMT[42] (2.86 g/cm$^3$). Overall the experimental compositions were found to vary by at most 1% from the theoretical values for weight percent inorganic content. In terms of physical properties, these samples remain relatively flexible even at the highest organoclay contents, as shown in Figure 1; likewise, all nanocomposite films can be easily bent, though they do tend to fracture if creased. While subsequent discussions will reference the organoclay content in percent by volume as a means of identifying the samples, volume fraction of inorganic material is the relevant composition variable as far as modeling is concerned.

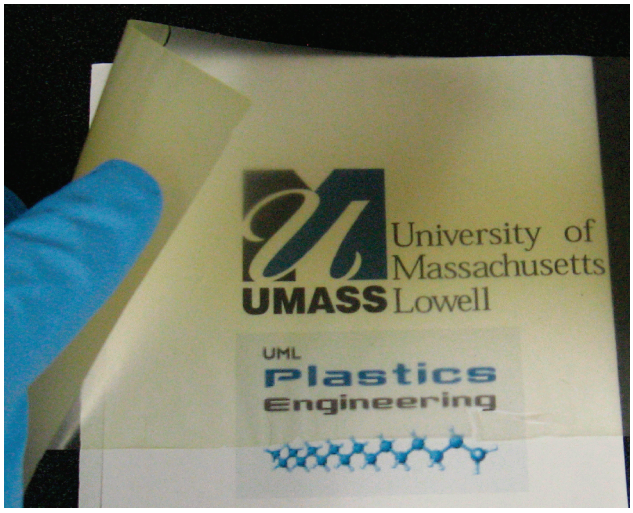


**Figure 1.** Sample containing 80 vol % DMDT-MMT demonstrating its flexibility and transparency.

In order to study nanocomposite morphology, 2D WAXD was chosen due to its ability to provide nanoscale structural information averaged over a representative volume of sample. A nanocomposite film was oriented parallel to the incident X-ray beam, producing a two-dimensional diffraction pattern (example shown in Figure 2) that was analyzed to determine both the interlayer spacing and the degree of orientation of the platelets (Table 1). An increase in interlayer spacing versus the pure organoclay film is indicative of polymer intercalation, while the orientation parameter is determined by performing an azimuthal scan of the second-order diffraction peak and calculating the Hermans orientation parameter.[43] This parameter ranges from −0.5 to 1, with a value of −0.5 in this case representing alignment of all

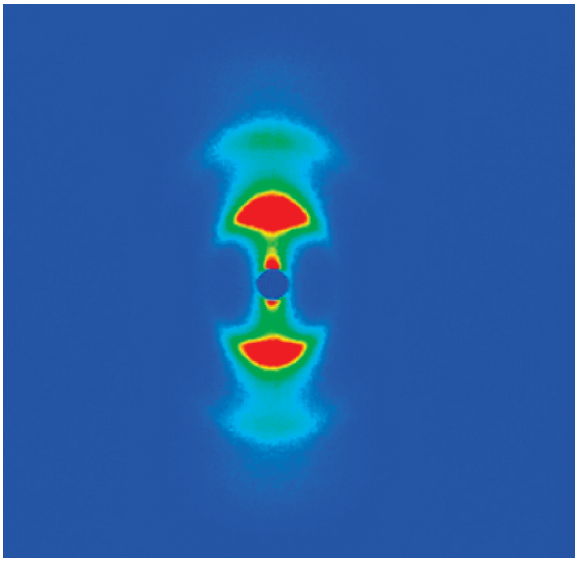

**Figure 2.** Example 2D WAXS pattern from a sample containing 70 vol % DMDT-MMT demonstrating radial intensity variations due to platelet orientation.

platelets perpendicular to the plane of the film, 1 representing alignment of all platelets in the plane of the film, and 0 representing random alignment with respect to the plane of the film. Measured orientation parameters ranged from 0.67 to 0.78 (Table 1), indicating a high level of orientation in the plane of the film. This is confirmed by examining freeze fractured edges of various samples via SEM (Figure 3). The SEM images show a well-ordered morphology consisting of well-defined parallel tactoids. The SEM also indicates a likely reason for why perfect alignment is not achieved. Examining the images closely reveals that while overall the tactoids are aligned, rippling is clearly evident. In WAXD, these ripples cause variations in the diffraction angle, resulting in the observed reduction in orientation parameter. WAXD also indicates polymer intercalation, with an increase in the interlayer spacing from 2.30 nm for pure DMDT-MMT to ~3.35 nm on average for the nanocomposites, as shown in Table 1, with an intermediate interlayer spacing of 2.79 nm observed in the polymer-starved 90 vol % DMDT-MMT sample.

The oxygen permeation data reported here shows that high aspect ratio fillers such as nanoclays can produce substantial improvements in barrier properties over the full range of compositions. As can be seen in Figure 4, adding nanoclay results an exponential reduction in oxygen permeability, with an order of magnitude decrease achieved by ~30 vol % organoclay. This result is likely due in part to the transition from isolated clay tactoids to a layered structure that would be expected at higher organoclay loadings.[44] At low organoclay loadings, tactoids are surrounded by significant quantities of neat polymer, and while the platelets themselves are able to slow permeating species, the surrounding polymer nevertheless allows for substantial permeation. As the organoclay content is increased, the tactoids begin to overlap more and more significantly, forming a layered structure with the polymer dispersed throughout. This layered structure contributes more effectively to the tortuous path effect that is often credited as the main source of the improvement seen with the addition of nanoclays. Once this structure has formed, further improvements arise from decreases in intertactoid spacing and increases in the number of layers per unit volume. Although there is ample evidence that the interphase will act differently than the bulk polymer in terms of its relaxation temperature, additional thermal analysis (MDSC and DMA, not shown), while providing evidence of some shift in the $T_g$ of the polystyrene to lower

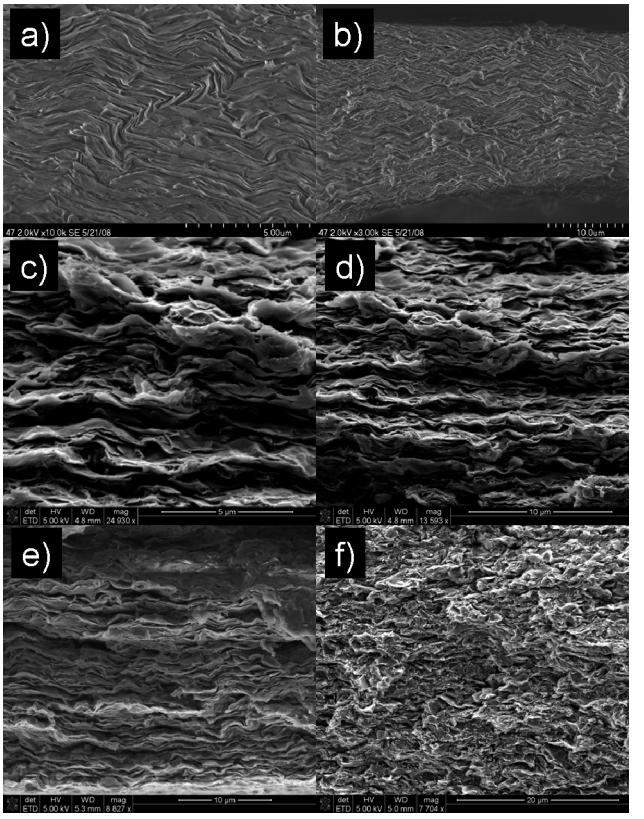


**Figure 3.** SEM images of neat DMDT-MMT at (a) high and (b) low magnification, of 40 vol % DMDT-MMT at (c) high and (d) low magnification, (e) of 80 vol % DMDT-MMT at low magnification, and (f) 20 vol % DMDT-MMT at low magnification, and (g) 2D WAXS and composite examples.

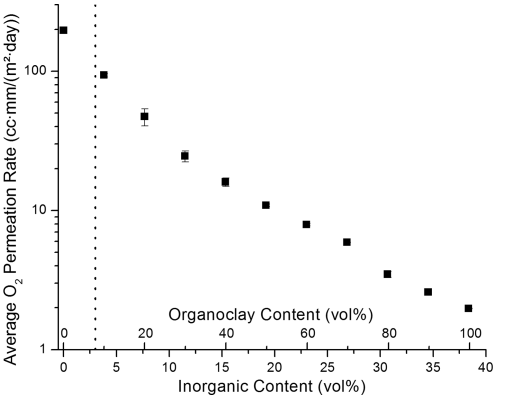


**Figure 4.** Experimental data for oxygen permeation in PS/DMDT-MMT nanocomposites, with tendency for exponential decay shown. The dashed line represents the center of the reported range[15,17] over which the transition from the dilute to the semidilute regimes is said to occur ($\alpha\varphi/\pi = 1$, where $\alpha$ is the layer aspect ratio and $\varphi$ is the volume fraction of layers).

temperatures, nevertheless confirms that the analysis temperature of 23 °C is below any thermal transitions in the material. In terms of overall segmental mobility, then, we can say that all organic components are below their lowest measurable thermal transition temperatures for the purposes of permeation analysis. A direct measurement of this effect should be possible if the clay layers could be oriented normal to the sample plane in a system right at the critical volume concentration for intercalation so as to avoid uncertainties associated with the tortuosity factor and focus solely on fundamental changes in diffusivity, but the preparation

of a material with this structure represents a significant challenge at this time.

The mathematical models often used to describe permeation in organoclay nanocomposites are based on a number of approaches. The simplest are the series and parallel coupling rule-of-mixtures approaches, which represent the upper and lower bounds in terms of barrier properties but are not applicable to materials containing discrete particles. The next level of detail relevant to the systems described here takes into consideration the presence of filler particles of a particular cross-sectional geometry and consequently represents a significant improvement. Such approaches describe the fillers as either ribbons/flakes (Nielsen[13] and Cussler[14]) or thin disks (Gusev and Lusti,[16] Fredrickson and Bicerano,[17] Cussler[15]). The results of the application of these approaches to our data are shown in Figure 5. Note that for this comparison the "random array" version of the Cussler model[15,45] was chosen to account for expected variations in tactoid spacing. As seen in Figure 5, all models are able to match the data over at least some part of the composition range explored here. One likely reason for the discrepancies observed, however, is that while the models account for platelet aspect ratio, they do not account for platelet orientation, and instead assume perfect alignment perpendicular to the direction of oxygen flow. As the orientation parameters listed in Table 1 make plain, even in highly aligned systems such as these, orientation is never perfect.

As mentioned previously, the method applied by Eitzmann, Melkot, and Cussler[19] and also by Bharadwaj to account for the effects of orientation on barrier properties in these systems[20] shows good agreement with simulation and experiment, with the

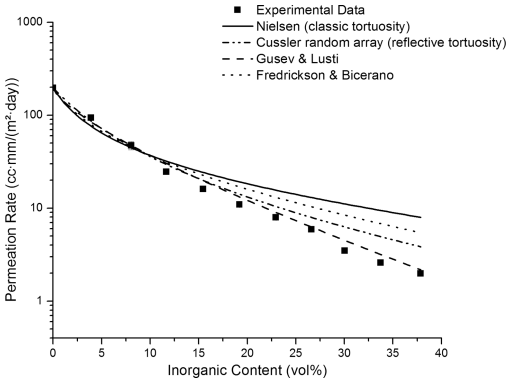


**Figure 5.** Experimental and model data for oxygen permeation rate in PS/DMDT-MMT nanocomposites (for coefficients of determination and fitting parameters refer to Table 3).

aforementioned approaches representing useful means of improving the applicability of the Cussler (regular array) and Nielsen models, respectively, to "real world" samples with nonideal levels of layer orientation. As we demonstrate, this approach can be equally applied to other models as well. All permeation models described here can be rearranged to isolate all of the tortuous path effects into a single term ($\tau$), giving eq 1 as a general result, where $P_0$ is the permeability of the neat polymer, $\phi$ is the volume fraction of the inorganic content, and $\tau$ is the geometric tortuosity factor. The Nielsen model,[13] for instance, could then be represented by inserting the Nielsen tortuosity factor shown in Table 2 into eq 1. Bharadwaj[20] extended the Nielsen model by including an orientation factor, S, as shown in eq 2, that was calculated to describe the overall orientation of the platelets. The orientation parameter allows for the calculation of a weighted average of the zero tortuosity and maximum tortuosity states, the latter being estimated by traditional permeation models. As with the Hermans orientation parameter,[43] the orientation parameter here also varies from $-0.5$ to 1. A value of $-0.5$ corresponds to platelet orientation parallel to the permeation direction and represents the zero tortuosity bound, where permeability is reduced only by a reduction in solubility due to the replacement of some amount of polymer by filler. A value of 1 corresponds to platelet orientation perpendicular to the permeation direction and represents the maximum tortuosity case, where all filler particles are perfectly oriented in-plane and perpendicular to the permeation direction. Finally, a value of 0 represents a state of random orientation. As this range of values implies, given the appropriate analytical geometries the orientation parameter defined by Bharadwaj and the Hermans orientation parameter defined for X-ray diffraction studies are equivalent. In support of this approach, it can also be seen that the orientation correction factor of $\cos^2\theta$ applied by Eitzmann, Melkot, and Cussler[19] is mathematically equivalent to the orientation correction of $(^2/_3)(S + {}^1/_2)$ applied by Bharadwaj, based on the definition of $S$, the Hermans orientation parameter, as $S = (3\cos^2\theta - 1)/2$.[46]

Generic permeation equation:

$$\frac{P_0}{P}(1-\varphi) = 1+\tau \tag{1}$$

Bharadwaj model[20] (Nielsen with orientation parameter):

$$\frac{P_0}{P}(1-\varphi) = 1+\left(\frac{\alpha\varphi}{2}\right)\left(\frac{2}{3}\right)\left(s+\frac{1}{2}\right) \tag{2}$$

The Bharadwaj approach represents an improvement over the classic Nielsen model, but is best applied to the dilute concen-

**Table 2. Published Formulas and Derived Tortuosity Factors for Various Barrier Models**

| model | original formula (as published) | tortuosity factor |
|---|---|---|
| classic tortuosity (Nielsen[13]) | $\frac{P_0}{P}(1-\phi) = 1+\frac{\alpha\phi}{2}$ | $\tau = \left(\frac{\alpha\phi}{2}\right)$ |
| reflective tortuosity (Cussler[2,15,45]) *regular array* | $\frac{P_0}{P}(1-\phi) = 1+\frac{(\alpha\phi)^2}{2}$ | $\tau = \frac{(\alpha\phi)^2}{2}$ |
| reflective tortuosity (Cussler[2,15,45]) *random array* | $\frac{P_0}{P}(1-\phi) = 1+\frac{2\alpha\phi}{3}+\frac{(\alpha\phi)^2}{9}$ | $\tau = \frac{2\alpha\phi}{3}+\frac{(\alpha\phi)^2}{9}$ |
| Gusev and Lusti[16] | $\frac{P_0}{P}(1-\phi) = e^{\left(\frac{\alpha\phi}{3.47}\right)^{0.71}}$ | $\tau = \left(e^{\left(\frac{\alpha\phi}{3.47}\right)^{0.71}}-1\right)$ |
| Fredrickson and Bicerano[17,45] | $\frac{P_0}{P}(1-\phi) = 4\left[\frac{(1+x+0.1245x^2)}{(2+x)^2}\right]^2$ where $x = \frac{\pi\alpha}{2\ln\left(\frac{\alpha}{2}\right)}$ | $\tau = \left(\frac{-1.01(2x+3)}{(x+2)^2+0.062x^2+0.748x+0.756}\right)$ |

tration regimes for which the Nielsen model was initially derived. In order to make use of this orientation-corrected approach more generally, we propose eq 3 as a generic form of the aforementioned approach, on the same basis as Bhardawaj's application to the Nielsen model[20] but stated in generalized form to allow for the use of tortuosity factors from any number of models. When the Nielsen tortuosity factor expressed in Table 2 is substituted into the generic orientation-corrected permeation model given as eq 3, the Bharadwaj model results. Along the same lines, the Cussler[15,45] tortuosity factor, derived for semidilute filler concentrations, can be combined with the orientation factor by inserting the tortuosity factor shown in Table 2 into eq 3 as well. The same goes for tortuosity factors derived from the Fredrickson and Bicerano[17] and Gusev and Lusti[16] models as well (Table 2).

Generic permeation equation with orientation parameter:

$$\frac{P_0}{P}(1-\varphi) = 1+\tau\left(\frac{2}{3}\right)\left(s+\frac{1}{2}\right) \quad (3)$$

Incorporating the orientation parameters measured via WAXD for each composition into the orientation-modified models described above (excepting the "regular array" Cussler model whose modification was previously reported in a different form by Eitzmann, Melkot, and Cussler,[19] as our materials are not regular by definition) gives the results shown in Figure 6. In Figure 6a, the models were fit to the data to generate the $P_o$, α, and $S$ values shown in Table 3, while in Figure 6b the plots were generated using actual measurements of the orientation parameter for each tested concentration in combination with the fitted values for $P_o$ and α for each model shown in Table 3. The $P_0$ for the neat PS used in this work was measured to be 196 $cm^3 \cdot mm/(m^2 \cdot day \cdot atm)$, similar to the literature value of 166 $cm^3 \cdot mm/(m^2 \cdot day \cdot atm)$[36,47] with the discrepancy observed ascribed to differences in process history and resin grade. It is noteworthy that, in spite of being allowed to vary to values as low as 0, the fitted values for α remain close to or within the manufacturer's stated range of 70−150[48] in all cases. Given the uncertainty regarding the exact shape of the aspect ratio distribution and the degree to which any fraction of that distribution might dominate the permeation behavior, we emphasize that it is not possible to identify any one aspect ratio value as "correct". With that said, based on these results we conclude that even in materials consisting of little more than intercalated tactoids, regardless of inorganic content the single platelet aspect ratio remains more influential than that of the much thicker intercalated stack to which it belongs. With the exception of the classic tortuosity approach, which was never intended to address filler concentrations as high as we report here and remains more or less unchanged following orientation correction, the introduction of the orientation parameter improves the fits of all of the models. As organoclay content increases, however, discrepancies between the models become more and more apparent, with the orientation-corrected "random array" Cussler[15,45] and orientation corrected Gusev and Lusti[16] matching the greatest range of data. Although the orientation corrected Gusev and Lusti trend line shifts away from the data slightly at the higher concentrations, it shifts closer at low concentrations reducing the range of the residual from approximately 14.5 to 5.5 and increasing $r^2$ value from 0.996 to 0.999 as shown in Table 2. This is consistent with the fact that the Cussler model was derived for semidilute systems and that the Gusev and Lusti model was based on FEM results covering values of $\alpha\varphi$ as high as 20.

The shift away from the models at higher concentrations is likely due to the shift to a polymer starved system where there is no longer sufficient polymer to intercalate into all of the organoclay galleries. The composition at which the system shifts from

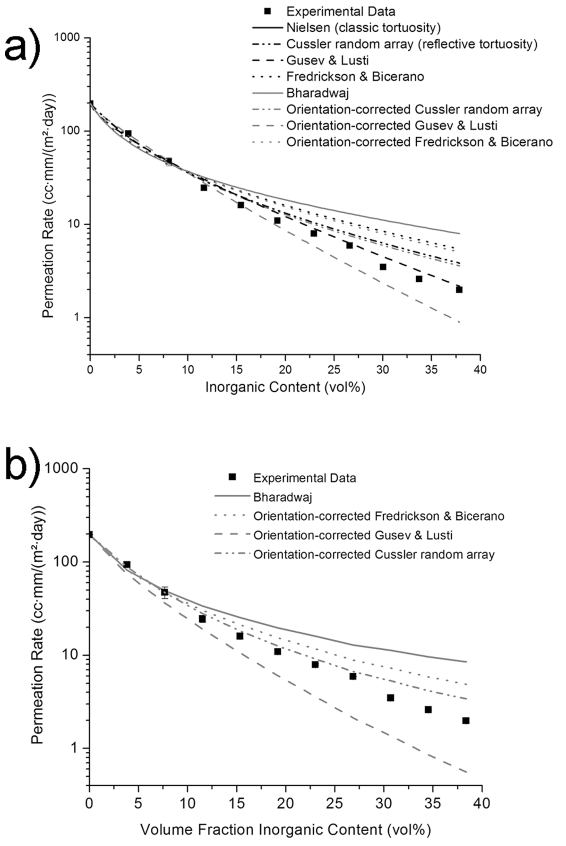


**Figure 6.** Orientation-corrected permeation models as applied to the PS/DMDT-MMT nanocomposite system, with (a) parameters fit to the data within realistic bounds and (b) results calculated using the measured permeability for pure polystyrene and the measured orientation parameters for each individual concentration.

polymer rich to polymer starved can be estimated by the ratio of the change in d-spacing due to polymer intercalation to the d-spacing of the neat organoclay and is found to be approximately 69.8 vol % DMDT-MMT (26.4 vol % inorganic) in this case. In the system containing 30 vol % polymer, effectively 100% of all organic material in the system consists of the so-called interphase, that is, an intimate mixture of intercalated polymer chains and clay modifiers. At lower polymer concentrations, unintercalated modifier will become more and more predominant. As such, it is legitimate to question whether $P_0$ may change when the system is polymer-starved. Rough estimates for $P_0$ of the intercalated interphase and unintercalated DMDT-MMT may therefore be made by applying the Gusev & Lusti models and Cussler random array (chosen based on their ability to describe a wide range of the data presented here) to materials containing 30 vol % and 0 vol % polymer, respectively. For these calculations, we use an aspect ratio of 70, this being the closest manufacturer-reported aspect ratio[48] to the best fit model values over the widest range of compositions. On the basis of this aspect ratio, the $P_0$ ranges for the intercalated interphase and unintercalated DMDT−MMT were found to be 223−426 and 231−318 $cm^3 \cdot mm/(m^2 \cdot day)$, respectively. While defining precise $P_0$ values for these phases would be premature given the various uncertainties with the modeling results, we can nevertheless state that they point to an inherent level of permeability similar to that of our neat polystyrene (197 $cm \cdot mm/(m^2 \cdot day)$). This helps to explain the success of these models even at the highest organoclay contents where the majority of the organic material present in the system consists of DMDT modifiers rather than polystyrene.

Exploring variations in orientation parameter reveals the model envelopes and provides another means to determine the

**Table 3. Adjusted Coefficient of Determinations and Fitted Parameters**

| | $r^2$ | $P_o$ | α | $S$ |
|---|---|---|---|---|
| Nielsen (classic tortuosity) | 0.976 | 197 ± 9.1 | 76.0 ± 11 | |
| Cussler random array (reflective tortuosity) | 0.996 | 197 ± 3.7 | 36.8 ± 1.7 | |
| Gusev and Lusti | 0.996 | 197 ± 3.8 | 65.2 ± 3.1 | |
| Fredrickson and Bicerano | 0.986 | 197 ± 6.9 | 83.3 ± 11 | |
| Bharadwaj (classic tortuosity) | 0.973 | 197 ± 9.7 | 88 ± 52 | 0.79 ± 760 |
| orientation-corrected Cussler random array (reflective tortuosity) | 0.997 | 197 ± 3.44 | 44.2.0 ± 17 | 0.67 ± 0.61 |
| orientation-corrected Gusev and Lusti | 0.999 | 197 ± 1.9 | 103 ± 7.7 | 0.77 ± 0.09 |
| orientation-corrected Fredrickson and Bicerano | 0.987 | 197 ± 6.8 | 111 ± 120 | 0.67 ± 1.09 |

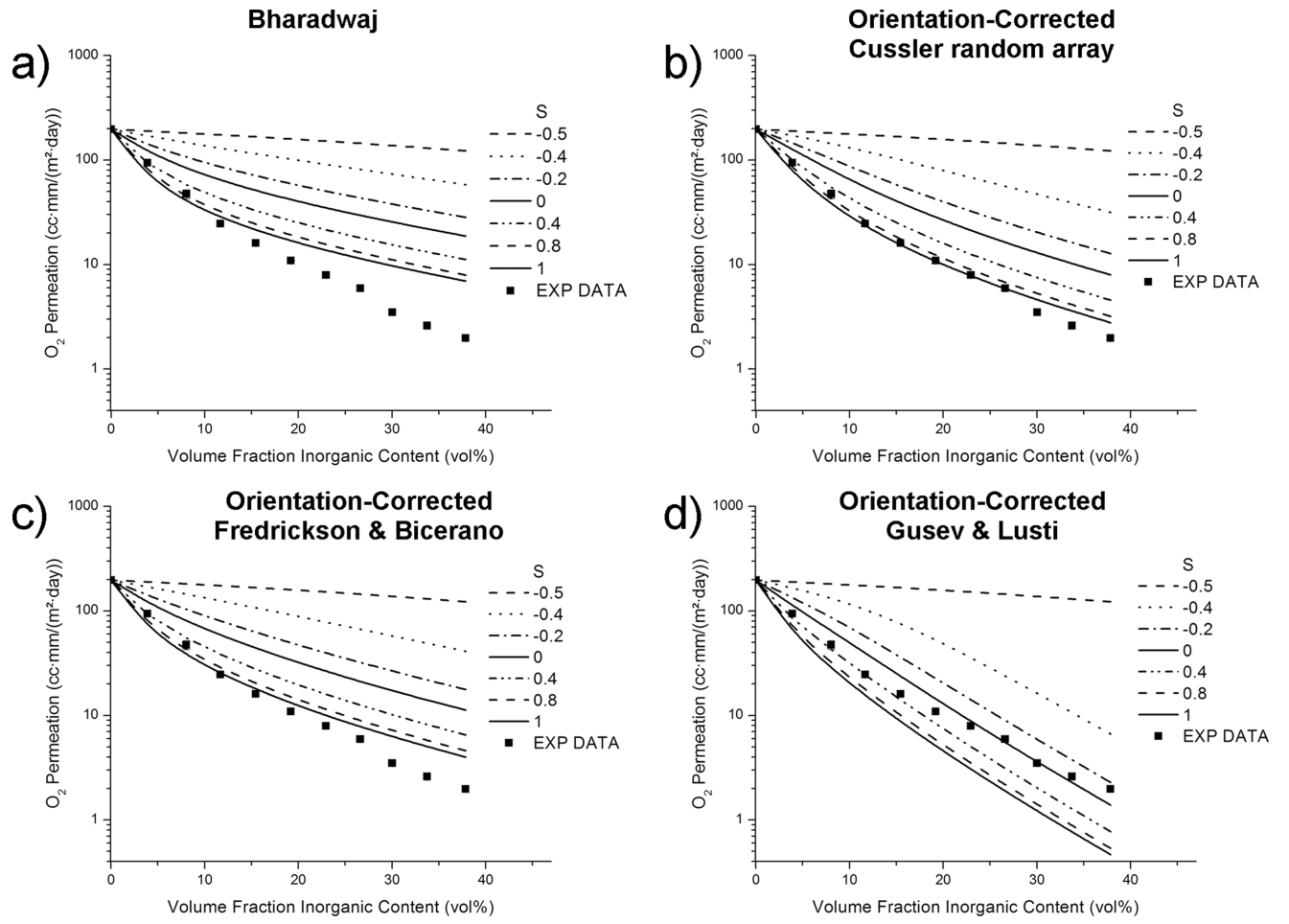


**Figure 7.** Orientation parameter ($S$) effects on the (a) Bharadwaj model, (b) orientation-corrected Cussler random array model, (c) orientation-corrected Fredrickson and Bicerano model and (d) orientation-corrected Gusev and Lusti model, using the aspect ratio (α) and the initial permeation rate ($P_o$) values fitted in Figure 6a and listed in Table 3.

range of applicability of a particular approach. Plots of the full range of orientation parameters for the four orientation-corrected models are shown in Figure 7. In this approach the aspect ratio (α) and the initial permeation rate ($P_o$) values were set to the fitted values determined in Figure 6a and listed in Table 3.

In all cases, a gradual increase in permeability is shown as the orientation parameter varies from one (perfect in-plane platelet orientation) to zero (random platelet orientation), with a more significant increase as the orientation parameter drops to −0.5 (perfect out-of-plane platelet orientation), extending the conclusions of Bharadwaj[20] regarding the effects of orientation to all of the models treated here. Likewise, these results also confirm that the classic tortuosity result (Nielsen,[13] Bharadwaj[20]) does indeed work best in the dilute regime, with deviations occurring over the range of concentrations predicted by Fredrickson and Bicerano as the limit of applicability of this approach.[17] Fredrickson and Bicareno's efforts[17] clearly improve on this result, matching the experimental data to a higher volume fraction of filler before deviating. The Gusev and Lusti envelope is the only one that encloses all of the data, though it does show the need for greater variations in orientation parameter than experimentally observed for a precise match. Finally, the Cussler random array envelope encloses most of the data and offers a close match over the entire composition range tested without the need for large variations in orientation parameter. In sum, these model envelope plots confirm the results shown in Figure 6 and Table 3, and add further detail in terms of the range of applicability of the various models studied.

The final portion of this study involves an investigation of the effects of temperature on the permeability of this system. Specifically, two samples, containing 50 vol % and 100 vol % DMDT-MMT, respectively, were tested at a series of temperatures ranging from 20 to 50 °C in 5 °C increments. Consistent with the behavior of pure polymers, increasing the temperature of the oxygen permeation analysis was observed to cause an exponential increase in the permeation rate. Following heating, a repeat

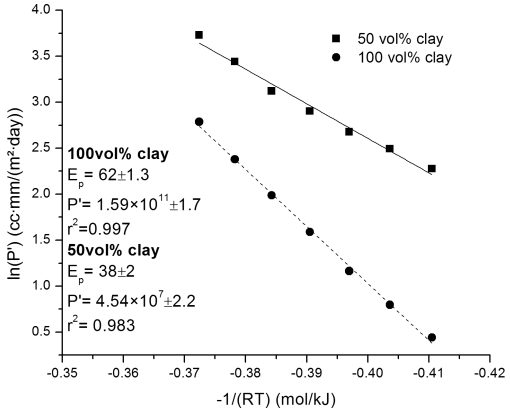


**Figure 8.** Arrhenius plots of the temperature dependence of the oxygen permeation rate in the PS/DMDT-MMT nanocomposite system.

analysis at 20 °C showed only a slight increase versus the first analysis at this temperature, confirming the reversibility of the effect observed. The resultant data (Figure 8) were fit to the Arrhenius relation expressed in eq 4, where *P'* is the exponential prefactor (measured in cm·mm/(m$^2$·day)), $E_P$ is the activation energy for permeation (in kJ/mol), *R* is the gas constant (8.314 J/(mol·K)) and *T* is the absolute temperature (K).

Arrhenius model for the temperature dependence of the permeation rate

$$P = P' e^{-E_P/RT} \tag{4}$$

These results are consistent with the well-known phenomenon whereby temperature affects the diffusivity and solubility of a permeant in a polymer. The organoclay modifier present in the 100 vol % DMDT-MMT sample exhibits this behavior as well, an anticipated result since the modifier is organic and would therefore be expected to show similar behavior to other permeable organic solids. Likewise, it is logical that the curve for the 100 vol % DMDT-MMT sample is well below that of the 50 vol % DMDT-MMT sample, given the expectation in the former case of both lower solubility (due to the higher inorganic content) and lower effective diffusivity (due to the tortuous path argument). It should be noted, however, that the organic phases here are compositionally different and changes in permeant solubility and tortuosity-independent diffusivity are likely to play at least some role given the differences in organic phase composition. In particular, the presence of thermal transitions above 23 °C but below that of bulk polystyrene[49] would be expected to result in increases in diffusivity with increased temperature above and beyond what is observed in bulk PS. That said, traversing a thermal transition should cause a change in the activation energy for permeation ($E_P$), whereas no evidence of such a change is seen in Figure 8. While the different slopes clearly reflect differences in the effective activation energies associated with permeation in these two materials further studies are needed to translate this observation into specific changes in sorption vs diffusion behavior. That said, these results support the conclusion that the effect of temperature on the barrier properties of organoclay nanocomposites depends both on the Arrhenius behavior of the organic phases present and tortuous path effects induced by the presence of the clay platelets.

## Conclusions

We report the preparation of a series of model nanocomposites based on polystyrene (PS) and dimethylditallowammonium montmorillonite (DMDT-MMT). The use of a novel spray casting technique allows for the preparation of free-standing films displaying high levels of uniformity and orientation, making them ideal barrier properties studies. Thermogravimetric analysis (TGA) confirms that the desired materials compositions were produced, while scanning electron microscopy (SEM) and wide-angle X-ray diffraction (WAXD) demonstrate the presence of a so-called "bricks and mortar" structure with a high degree of regularity and orientation regardless of organoclay content.

The oxygen permeation rate of these materials has been shown to decrease consistently and predictably with the addition of organoclay. The importance of orientation is shown through the application of an orientation correction to all of the modeling approaches used, and the range of applicability of each approach is identified both through direct fitting with appropriately constrained fitting parameters and envelope plots indicating if and when the experimental results are "out of bounds" for a particular model. On the basis of these results, the applicability of classic tortuosity approach (Nielsen,[13] Bharadwaj[20]) to the dilute regime is confirmed, with deviations occurring over the range of compositions predicted by Fredrickson and Bicerano[17] and reduced in magnitude using the latter authors' approach. The orientation-corrected Gusev and Lusti model shows its ability to capture all of the experimental data within its envelope, producing a good fit especially in the dilute concentration regime. Finally, while the orientation-corrected random array Cussler random array[15,45] model only captures most of the experimental data in its envelope, it is able to do so without need for significant variations in orientation parameter. In addition to highlighting the strengths of each approach, our extension of several of these models to include an orientation parameter further emphasizes the importance of orientation as far as the barrier properties of layered silicate nanocomposites are concerned.

Beyond tortuous path effects, the consequences of changes in temperature on the barrier properties of selected materials are shown to match well with the Arrhenius behavior frequently observed in neat polymers, even when no polymer is present in the material in question. This study allows us to quantify the sensitivity of the organoclay modifier to Arrhenius effects as far as barrier properties are concerned, adding to our understanding of the determinants of barrier properties in polymer nanocomposites based on such materials.

In sum, we present the first report comparing results from all major barrier properties models applied to platelet-based polymer nanocomposites with experimental data covering all possible compositions in an ideal model system. Building on the work of Eitzman, Melkote, and Cussler[19] and that of Bharadwaj,[20] we present a generic approach to the orientation correction of any barrier properties model and demonstrate its utility in practice. In addition to presenting model envelopes and identifying and attempting to explain ranges of applicability, we propose a method of estimating $P_0$ values for the interphase and the clay modifier and quantify the effects of temperature in these systems as well. While only one polymer has been used in this work, systems with other polymers are currently being investigated to confirm the generality of this approach, with preliminary data supportive of the aforementioned conclusions. The results reported here extend our knowledge of the barrier properties of polymer/organoclay nanocomposites, with clear implications for their design and application.

**Acknowledgment.** We thank Hilmar Koerner, Gary Price and Scott Fillery at the United States Air Force Research Laboratory (WPAFB, OH) for assistance with XRD and SEM analysis and for providing helpful feedback, as well as Richard Vaia and his group for general support, assistance, and facilities access. We thank the NSF-sponsored Center for High-Rate Nanomanufacturing at UML for access to the thermal analysis equipment, the UML Baseball Research Laboratory for sample conditioning facilities, and the Department of Plastics Engineering

for general support. Finally, we would like to thank the United States Air Force Laboratory and the Universal Technology Corporation for providing the financial support that made this work possible.

**Supporting Information Available:** Text discussing experimental procedured and a figure showing TGA comparisons for films. This material is available free of charge via the Internet at http://pubs.acs.org.

## References and Notes

(1) Picard, E.; Vermogen, A.; Gerard, J.; Espuche, E. *J. Membr. Sci.* **2007**, *292*, 133.
(2) Sun, L.; Boo, W.; Clearfield, A.; Sue, H.; Pham, H. *J. Membr. Sci.* **2008**, *318*, 129.
(3) DeRocher, J. P.; Gettelfinger, B. T.; Wang, J.; Nuxoll, E. E.; Cussler, E. *J. Membr. Sci.* **2005**, *254*, 21–30.
(4) Falla, W. R.; Mulski, M.; Cussler, E. L. *J. Membr. Sci.* **1996**, *119*, 129.
(5) Zhong, Y.; Janes, D.; Zheng, Y.; Hetzer, M.; Kee, D. D. *Polym. Eng. Sci.* **2007**, *47*, 1101.
(6) Heinz, H.; Vaia, R. A.; Krishnamoorti, R.; Farmer, B. L. *Chem. Mater.* **2007**, *19*, 59.
(7) Feeney, C. A.; Farrell, M.; Tannert, K.; Goldberg, H. A.; Lu, M.; Grah, M. D.; Steiner, W. G.; Winston. U.S. Patent 6,087,016, 2000.
(8) Feeney, C. A.; Goldberg, H. A.; Farrel, M.; Karim, D. P.; Oree, K. R. U.S. Patent 7,078,453, 2006
(9) Jang, W.; Rawson, I.; Grunlan, J. C. *Thin Solid Films* **2008**, *516*, 4819.
(10) Shim, B. S.; Podsiadlo, P.; Lilly, D. G.; Agarwal, A. *Nano Lett.* **2007**, *7*, 3266.
(11) Bonderer, L. J.; Studart, A. R.; Gauckler, L. J. *Science* **2008**, *319*, 1069.
(12) Ward, I. M.; Sweeney, J. *An Introduction to the Mechanical Properties of Solid Polymers*; 2nd ed.; Wiley: West Sussex, England, 2004.
(13) Nielsen, L. *J. Macromol. Sci.* **1967**, *5*, 929.
(14) Cussler, E.; Hughes, S. E.; Ward, W. J., III; Aris, R. *J. Membr. Sci.* **1988**, *38*, 161.
(15) Lape, N. K.; Nuxoll, E. E.; Cussler, E. L. *J. Membr. Sci.* **2004**, *236*, 29–37.
(16) Gusev, A. A.; Lusti, H. R. *Adv. Mater.* **2001**, *13*, 1641.
(17) Fredrickson, G. H.; Bicerano, J. *J. Chem. Phys.* **1999**, *110*, 2181.
(18) Cole, K. C.; Perrin-Sarazin, F.; Dorval-Douville, G. *Macromol. Symp.* **2005**, *230*, 1.
(19) Eitzman, D. M.; Melkote, R. R.; Cussler, E. L. *AIChE J.* **1996**, *42*, 2.
(20) Bharadwaj, R. K. *Macromolecules* **2001**, *34*, 9189.
(21) Vaia, R. A.; Liu, W.; Koerner, H. *J. Polym. Sci., Part B: Polym. Phys.* **2003**, *41*, 3214.
(22) Ho, D. L.; Briber, R. M.; Glinka, C. J. *Chem. Mater.* **2001**, *13*, 1923.
(23) Ho, D. L.; Glinka, C. J. *Chem. Mater.* **2003**, *15*, 1309.
(24) Fu, X.; Qutubuddin, S. *Mater. Lett.* **2000**, *42*, 12.
(25) Yilmazer, U.; Ozden, G. *Polym. Compos.* **2006**, *27*, 249.
(26) Noh, M. W.; Lee, D. C. *Polym. Bull.* **1999**, *42*, 619.
(27) Doh, J. G.; Cho, I. *Polym. Bull.* **1998**, *41*, 511.
(28) Zhong, Y.; Zhu, Z.; Wang, S. *Polymer* **2005**, *46*, 3006.
(29) Salahuddin, N.; Akelah, A. *Polym. Adv. Technol.* **2002**, *13*, 339.
(30) Uthirakumar, P.; Hahn, Y. B.; Nahm, K. S.; Lee, Y. *Eur. Polym. J.* **2005**, *41*, 1582.
(31) Hoffmann, B.; Dietrich, C.; Thomann, R.; Friedrich, C.; Mulhaupt, R. *Macromol. Rapid Commun.* **2000**, *21*, 57.
(32) Ding, C.; Guo, B.; He, H.; Jia, D.; Hong, H. *Eur. Polym. J.* **2005**, *41*, 1781.
(33) Zax, D. B.; Yang, D.; Santos, R. A.; Hegemann, H.; Giannelis, E. P.; Manias, E. *J. Chem. Phys.* **2000**, *112*, 2945.
(34) Vaia, R. A.; Jandt, K. D.; Kramer, E. J.; Giannelis, E. P. *Macromolecules* **1995**, *28*, 8080.
(35) Hong, S.; Krochta, J. M. *J. Food Eng.* **2006**, *77*, 739.
(36) Brandrup, J.; Immergut, E. H.; Grulke, E. A. *The Polymer Handbook*; 4th ed.; John Wiley & Sons: New York, 1999.
(37) Dunkerley, E.; Schmidt, D. Stiff, Highly Damping Thermoplastic Polyurethane Nanocomposites via Simple, Scalable Processing. In *67th ANTEC 2009 Plastics: Annual Technical Conference Proceedings*, Chicago, IL, June 22−24, 2009; Society of Plastics Engineers: Brookfield, CT, **2009**; p 92.
(38) Dunkerley, E.; Schmidt, D. The Optimization of High Inorganic Content Hybrid Barrier Materials. In *68th ANTEC 2010 Plastics: Annual Technical Conference Proceedings*, Orlando, FL, May 16−20, 2010; Society of Plastics Engineers: Brookfield, CT, **2010**; p 702.
(39) Dunkerley, E.; Schmidt, D. *Abstracts of Papers, 240th ACS National Meeting*; American Chemical Society: Washington, DC, **2010**; PMSE-336.
(40) Scientific Polymer, http://www.scientificpolymer.com/catalog/description.asp?QProductCode=845, viewed 10/2010.
(41) Southern Clay Products, http://www.scprod.com/product_bulletins/PB%20Cloisite%2020A.pdf, viewed 10/2010.
(42) Southern Clay Products. http://www.scprod.com/product_bulletins/PB%20Cloisite%20NA+.pdf, viewed 10/2010.
(43) Yoonessi, M.; Toghiani, H.; Pittman, C. U. *J. Appl. Polym. Sci.* **2006**, *102*, 2743.
(44) Hbaieb, K.; Wang, Q.; Chia, Y.; Cotterell, B. *Polymer* **2007**, *48*, 901.
(45) Takahashi, S.; Goldberg, H.; Feeney, C.; Karim, D.; Farrell, M.; O'Leary, K.; Paul, D. *Polymer* **2006**, *47*, 3083–3093.
(46) Gedde, U. W. *Polymer physics*; Springer: Berlin, 1995.
(47) Salame, M. *J. Polym. Sci. Symp.* **1973**, *41*, 1.
(48) Organoclays Nanoclay Additives for Reinforced Plastics, http://www.nanoclay.com/benefits.asp, viewed 10/2010.
(49) Jacobs, J. D.; Koerner, H.; Heinz, H.; Farmer, B. L.; Mirau, P.; Garrett, P. H.; Vaia, R. A. *J. Phys. Chem. B* **2006**, *110*, 20143.